

Denudation rates across the Pamir based on ^{10}Be concentrations in fluvial sediments: Dominance of topographic over climatic factors

Margret C. Fuchs^{1,2}, Richard Gloaguen^{1,2}, Silke Merchel³, Eric Pohl¹, Vasila A. Sulaymonova¹, Christoff Andermann⁴, and Georg Rugel³

¹Remote Sensing Group, Institute of Geology, TU Bergakademie Freiberg, Bernhard-von-Cotta-Strasse 2, 09599 Freiberg, Germany

²Helmholtz-Zentrum Dresden-Rossendorf, Helmholtz Institute Freiberg for Resource Technology, Remote Sensing Group, Halsbrücker Strasse 34, 09599 Freiberg, Germany

³Helmholtz-Zentrum Dresden-Rossendorf, Helmholtz Institute Freiberg for Resource Technology, Bautzner Landstrasse 400, 01328 Dresden, Germany

⁴Section 5.1 Geomorphology, German Research Centre for Geoscience GFZ, Telegraphenberg, 14473 Potsdam, Germany

Correspondence to: Margret C. Fuchs (fuchsm@mailserver.tu-freiberg.de)

Abstract.

A clear understanding of erosion processes is fundamental to study the evolution of actively deforming mountain ranges, whereas the relative contributions of tectonic and climatic factors and their feedbacks remain highly debated. The Pamir is peculiar in both, high deformation rates induced by the India-Eurasia collision and its position at the transition between Westerlies and Monsoon. In order to contribute to this debate we quantify basin-wide denudation rates from cosmogenic ^{10}Be concentrations in modern river sediments measured by accelerator mass spectrometry. The sample acquisition is logistically demanding and preparation was challenging due to low quartz and high feldspar concentrations as well as crystal coating. Sample locations represent the Panj basin at six sites along its trunk stream, and the major, east-west elongated tributary basins at five sites. An average denudation rate of ~ 0.64 mm/yr for the entire Pamir reveals a rapid landscape evolution. Denudation rates of tributary sub-basins highlight the strong contrast between the Pamir Plateau (0.05 mm/yr to 0.16 mm/yr) and its margins (0.54 mm/yr to 1.45 mm/yr).

The intensity of denudation is primarily correlated to geometric properties of the surface such as slope steepness (0.75 quartiles; R^2 of 0.81) and to a much lesser extent to climatic factors such as precipitation. We thus argue that either tectonic uplift or base level lowering are the main contributors to denudation processes. Multiple linear regression analysis (best R^2 of 0.93) reveals that precipitation may contribute to the efficiency of denudation as a limiting factor. The highest rates coincide with areas that receive precipitation predominantly from the Westerlies during winter. The concentrated discharge during spring and early summer may favour the pronounced denudation along the

north-western Pamir margin by driving the sediment flux out of the basins. Low slope angles and dry conditions are unfavourable for sediment transport and consequently, denudation on the plateau. The magnitude of denudation in the Pamir is similar to rates determined in the south Himalayan escarpment, whereas climatic and tectonic conditions are very different. The discrepancy between rates of basin-wide denudation and up to ten times higher fluvial incision at the Pamir margins evidences a transient landscape. This comfort the hypothesis that river captures are responsible for the strong base level drop driving the incision along the Panj. The uplifted landscape and fast incision preserve steep hillslopes that allow high rates of denudation at the Pamir margins. Winter precipitations may act as a limiting factor to hillslope adjustment and consequently, to denudation processes.

30 **1 Introduction**

The rapid evolution of active mountain chains depends on complex interactions between tectonically triggered rock uplift and climate-driven processes (e.g. Montgomery and Brandon, 2002; Burbank et al., 2003; Huntington et al., 2006; Godard et al., 2012, 2014). The variable in situ conditions imply spatial and temporal variations of erosion rates that may allow to constrain the role of tectonics and climate on mountain evolution and vice versa, for example when erosion induces mass loss that will be compensated by isostatic rebound (e.g. Molnar and England, 1990; Burbank and Anderson, 2000; Champagnac et al., 2009). The wealth of erosion data available in the India-Asia orogenic belt concern mainly the southern escarpment of the Himalayas and focus on the coupling of tectonic uplift and the intensity of the ISM. The Pamir is much drier and influenced by the Westerlies that provide most precipitation during winter (and spring) as snow (Pohl et al., 2014, under review).

Short-term or small-scale erosion rates are not yet available for the Pamir, but are needed to understand the role of differential tectonics and the climatic gradients on the magnitude of erosion, and how much erosion estimates vary depending on the captured time interval (e.g. Garzanti et al., 2007; Lupker et al., 2012). Additionally, the comparison to other studied sites of the India-Asia collision zone may deliver new insights into the mechanisms of erosion under variable conditions. The tectonic and climatic setting of the Pamir provides ideal conditions to study erosion in response to variable drivers. The orogen lies at the westernmost part of the India-Asia collision zone, one of the Earth's largest and most rapidly deforming intra-continental convergence zone (e.g. Reigber et al., 2001; Mohadjer et al., 2010). This position coincides with the transition between the atmospheric circulation systems of the Indian Summer Monsoon (ISM) and the Westerlies, making this region particularly interesting when studying the role of climate on mountain evolution. The magnitude of erosion, its spatial and temporal variations and how tectonics and climate interact are poorly constrained in the Pamir. Erosion was only studied in the context of the tectonic evolution of the Pamir. This includes the study of active tectonic dome formation in the southern Pamir, in which Stübner et al. (2013) inferred roughly 0.5 mm/yr erosion during the Miocene from thermochronological mod-

elling of the exhumation and geometric reconstructions of the Shakh dara Dome. Carrapa et al. (2014) suggest a regional exhumation gradient of the Pamir with about 0.2 mm/yr in the northeast and between 0.6 mm/yr and above 2.0 mm/yr in central and southern Pamir during the Miocene-Pliocene. They attribute the gradient to differing precipitation quantities that may cause much higher erosion rates in western marginal parts of the orogen. Such long-term and somehow contradictory erosion rates inferred from exhumation reconstruction integrate over variable climatic conditions during several million years and cannot resolve spatial variations of the erosional response to climatic gradients or changes in uplift across the Pamir below the regional scale.

In the Himalaya, variations in erosion were found to correlate to long-term climate fluctuations that govern glacial processes (Gabet et al., 2008; Godard et al., 2012) and the intensity of the ISM (e.g. Bookhagen et al., 2005). Links between precipitation and erosion correspond also to regional relief characteristics that induce orographic effects (e.g. Garzanti et al., 2007; Gabet et al., 2008). Orographic rain shadow leads to a shift from precipitation- to temperature-sensitive erosion across the southern Himalayan escarpment resulting in an increased influence of concentrated peak discharge during the melting season on erosion (e.g. Burbank et al., 2012). Additionally, the availability of sediment to be transported (Burbank et al., 2012) and the magnitude-frequency distribution of direct runoff (Andermann et al., 2012) modulate rates of erosion. The generation of sediment and direct runoff are genetically linked to slope or relief as a consequence of base level lowering, hillslope thresholds or landslide frequency, factors that were found to control erosion (e.g. Montgomery and Brandon, 2002; Ouimet et al., 2009). In particular, the correlation between erosion and long-term tectonic uplift in the Greater Himalaya is debated as rates are suggested to adjust fast to climatic variations (Burbank et al., 2003; Godard et al., 2014).

In this study, we aim at determining the magnitude of denudation in the Pamir at the time-scale of 10^2 yr to 10^4 yr using ^{10}Be concentrations in quartz of active river channel sediments. We analyze eleven samples of the Panj river network to resolve the spatial variations of denudation rates for all major sub-basins as well as record changes with increasing basin sizes along the trunk river. Sampled polymineral sediments required extensive preparation techniques to extract Be from pure quartz and to measure the long-lived cosmogenic radionuclide ^{10}Be by accelerator mass spectrometry at DREAMS (Akhmadaliev et al., 2013). Calculated production rates and shielding factors represent basins upstream of each sampling site. We analyze the variations in basin-wide denudation rates using (multiple) linear regression analysis including geomorphic (altitude, relief, slope) and climatic (snow and ice cover, and precipitation) basin parameters and discuss the influence of spatial and temporal averaging. This contribution focusses on the first denudation rates measured in the Pamir and their implications for our understanding of surface processes in that region. This paper is a distinct addition to previous works (Fuchs et al., 2013, 2014) based on OSL dating of river terraces and geomorphic indicators that have shown the response of the Panj drainage system to tectonics, i.e.

incision rate variability related to main tectonic structures in the Pamir and a possible re-organization of the Panj drainage system.

2 Regional setting

95 2.1 Geological setting

The Pamir is located at the northwestern end of the India-Asia collision zone. The series of sutures, magmatic belts and crustal blocks are assumed to consist of along-strike equivalents of the Tibetan Plateau that accreted to the Eurasian plate during the Paleozoic to Mesozoic (e.g. Burtman and Molnar, 1993; Schwab et al., 2004; Cowgill, 2010; Bershaw et al., 2012). The main tectonic structures allow the distinction between three distinct terranes: the Northern, Central, and Southern Pamir (Burtman and Molnar, 1993; Schwab et al., 2004). Cenozoic domes cover up to 30% of the Pamir and comprise a steady-state elevated plateau (Ducea et al., 2003; Schwab et al., 2004; Schmidt et al., 2011; Stübner et al., 2013). The structural domes (Fig. 1A) expose Cretaceous arc-type granitoids, mantled by lower-grade to non-metamorphic rocks (Schwab et al., 2004; Robinson, 2009; Schmidt et al., 2011; Stübner et al., 2013). The northern Kurgovat Dome consists of high-grade metamorphosed Triassic rocks. The central Yazgulom, Sarez, Muskol, Shatput and the southern Shakhdara and Alichur Domes exhumed high-grade metamorphic rocks of Oligocene to Miocene ages with peak exhumation at ~ 15 Myr (Schmidt et al., 2011; Stübner et al., 2013).

The active frontal range of Pamir bends nearly 180° from northern Afghanistan to western China (Bershaw et al., 2012). Neotectonic activity is governed by the northward propagation of the Indian plate inducing east-west striking mountain ranges. Crustal shortening is mainly accommodated at the Main Pamir Thrust (MPT) by subduction beneath the frontal part of the orogen where most of the seismicity occurs (e.g. Koulakov and Sobolev, 2006; Schneider et al., 2013; Sippl et al., 2013). Recently published shortening rates reach 10 - 15 mm/yr across the MPT (Ischuk et al., 2013). The lateral margins of the orocline display strike-slip motion of ~ 12 mm/yr along the western Darvaz Fault Zone (DFZ) (Trifonov, 1978; Mohadjer et al., 2010) and < 1 mm/yr along the eastern Karakoram Fault Zone (KFZ) (Strecker et al., 1995). The Southern Pamir Shear Zone (SPSZ) delineates the Pamir to the south from the Hindu Kush. This major east-west, low-angle normal fault comprises the southern boundary of the giant Shakhdara Dome. Plateau-internal neotectonic seismicity is related to the gravity driven collapse of the Plateau and the induced east-west extension and conjugated strike-slip (Fan et al., 1994; Strecker et al., 1995; Sippl et al., 2013)

2.2 Climatic setting

The position of the Pamir at the transition between the Westerlies and the ISM makes the region highly sensitive to variations in atmospheric circulation patterns. Tropical Rainfall Measurement Mission (TRMM) spatial product 3B42 V7 (Huffman et al., 1997, 2007) reveals strong variations of

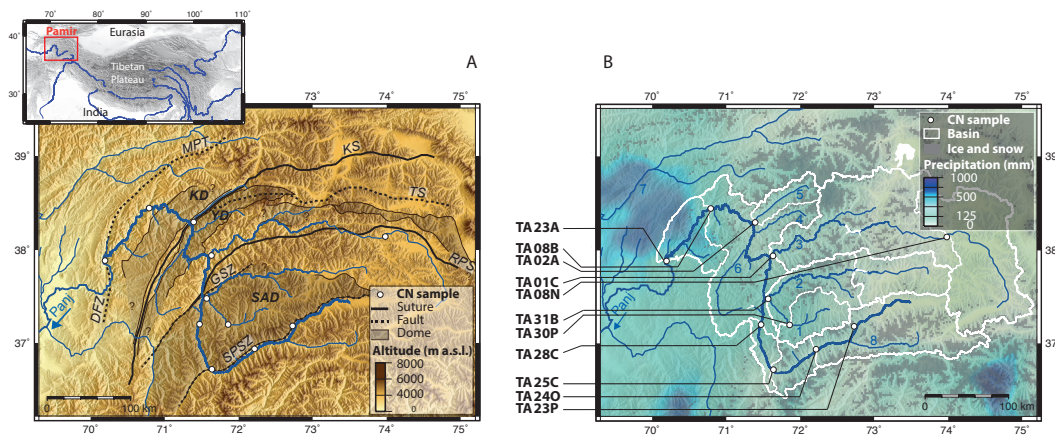


Figure 1. Regional setting of the Pamir river system and sample locations (CN: cosmogenic nuclide, a.s.l.: above sea level). A: Topography and main tectonic structures (DFZ: Darvaz Fault Zone, MPT: Main Pamir Thrust, KS: Kunlun Suture, TS: Tanymas Suture, RPS: Rushan-Psart Suture, GSZ: Gunt Shear Zone, SPSZ: Southern Pamir Shear Zone, KD: Kurgovat Dome, YD: Yazgulom Dome, SAD: Shakh dara and Alichur Dome, modified after e.g., Schwab et al., 2004; Stübner et al., 2013). B: Sample locations along the Panj and major tributaries (1: Shakh dara, 2: Gunt, 3: Bartang, 4: Yazgulom, 5: Vanj, 6: Shiva, 7: Vakhsh, 8: Wakhan) and related drainage basins. The climate is shown by the distribution of annual precipitation (TRMM 3B42 V7, 1998-2012, Huffman et al., 1997, 2007) and permanent snow and ice cover (MODIS MCD12Q1, Strahler et al., 1999, year 2010).

annual precipitations (mean 1998 - 2012) from almost nil to more than 500 mm in Pamir (Fig. 1B). The Westerlies supply precipitation during winter and spring to the north-western Pamir margins. The precipitation from the south during the ISM strongly attenuates over the Hindu Kush and Karakoram Range. The central Pamir receives very little annual precipitation, mainly in form of snow. The westward increase of permanent snow and ice cover (Moderate Resolution Imaging Spectrometer, MCD12Q1, version 057, 2010, Strahler et al. (1999)) illustrates the superimposition of concentrated precipitation at the Pamir margins and low temperature due to high altitudes (Fig. 1B).

Past fluctuations of glacial extents may affect erosion and sediment yields dependent on the averaging time. Glacial remnants attest for significant climatic variations during the Late Quaternary on the Pamir Plateau. Successively less extensive glacial advances correspond to an increasing aridity in Central Asia (Zech et al., 2005; Abramowski et al., 2006; Röhringer et al., 2012). Beryllium-10-based dating of moraines on the Pamir Plateau puts the most extensive glaciation during the marine isotope stage (MIS) 4 or earlier, during MIS 5 to MIS 6. The glaciers of this most extensive glacial advance reached the inner-plateau valley floors 136-93 kyr and 86-60 kyr ago. A potential ISM driven MIS 3 advance related to hummocky moraines is ambiguous due to high age scatter. Two less extensive advances are dated at 30-27 kyr (MIS 3/MIS 2) and 24-22 kyr (MIS 2). Younger glacial sediments are associated to de-glaciation or minor re-advances.

3 Material and methods

3.1 Beryllium-10-based modern denudation rates

145 Beryllium-10 concentrations in modern fluvial sediments are inversely proportional to the rate of
landscape lowering by weathering and physical erosion and average the exposure time of rock sur-
faces to cosmic ray interaction (von Blanckenburg, 2005; Dunai, 2010). The generally dry conditions
in Pamir (Fig. 1) suggest weathering to be of less importance in the total erosion budget. In this case,
150 means that denudation rates narrow down to erosion rates (e.g. Dunai, 2010), and it may be con-
venient to use both terms interchangeably in the following and when comparing rates across time
scales.

The ^{10}Be concentration C in quartz is inversely proportional to the denudation rate ε (Lal, 1991;
Brown et al., 1995; von Blanckenburg, 2005) and can be described by:

$$155 \quad \varepsilon = \left(\frac{P}{C} - \lambda \right) * z^* \quad (1)$$

where λ is the decay constant of the nuclide and P its production rate. To calculate λ by

$$\lambda = \frac{\ln(2)}{t_{1/2}} \quad (2)$$

we used the ^{10}Be half-life ($t_{1/2}$) of (1.387 ± 0.012) Myr (Korschinek et al., 2010). For the atten-
uation depth z^* , we used 60 cm to represent silicate rocks (Lal, 1991; von Blanckenburg, 2005).
160 Assuming constant ^{10}Be production and material removal at the surface, the measured nuclide con-
centration, and hence, the denudation rate, averages over the time (T_{ave}) it takes to erode z^* and
hence, to remove the ‘cosmogenic memory’ of the material (Brown et al., 1995; Bierman and Steig,
1996; von Blanckenburg, 2005; Dunai, 2010). For further details see the supplementary material.

3.2 Sampling strategy

165 We sampled 11 locations of the Panj river network (Fig. 1B). Five sampling sites represent the in-
creasing basin along the trunk river reach of the Panj until it crosses the DFZ. Three major tributaries
(Gunt, Bartang and Vanj River, Fig. 1B) were sampled near their confluence with the Panj and three
additional sites were selected to represent upstream sub-basins. This relatively low number of sam-
ples is explained by the fairly difficult accessibility of the region. Additionally, difficulties to find
170 suitable sites of modern fluvial sediments arose from the high stream power of the Panj that limits
the deposition of sand in Pamir.

We chose locations before confluences as far as possible from upstream tributaries, to ensure
complete mixing of sediment grains that are representative for all upstream source areas. Locations

have been avoided where slope failure or fan sedimentation from minor tributaries indicated local
175 perturbations. We sampled directly the uppermost 1 - 3 cm of the sediment in the active river channel.
All samples consisted of predominantly sand-sized, polymineral material. Sufficient material for
quartz and subsequent ^{10}Be extraction was addressed by collecting 3 - 5 kg of fluvial sediment per
sample.

3.3 Sample preparation and ^{10}Be measurements

180 The polymineral sediment samples showed relatively low quartz but high feldspar contents as well as
mineral coatings and hence, required quartz enrichment before starting chemical cleaning and ^{10}Be
extraction. Quartz enrichment included wet sieving (focus on 250 - 500 μm , for samples TA28C and
TA30P only the coarser fraction 500 - 1000 μm yielded sufficient material), magnetic separation and
ultrasonic bath. Repeated cleaning of the quartz with a 1:1 solution of HCl (32%) and H_2SiF_6 (34%)
185 (Brown et al., 1991) was insufficient to diminish the feldspar (up to 50 %). Such feldspar contents
may cause bias in quartz results due to differing rates of ^{10}Be production, as well as lower chemical
resistance and high aluminum contents that affect chemical procedures. Therefore, we introduced
feldspar flotation to separate pure quartz (Herber, 1969). The feldspar flotation was carried out in
a solution of 0.2% HF and pH of 2.4 - 2.7 to activate feldspar adherence to bubbles using the foam
190 agent dodecylamine.

Atmospheric ^{10}Be was removed by dissolving 30% of the extracted quartz fraction with 48% HF
during three cycles. The BeO separation and Be extraction followed the procedures by Merchel and
Herpers (1999) (for details see the supplementary material). We added about 300 μg of a ^9Be carrier
(Phena DD, $(3.025 \pm 0.009) \times 10^{-3} \text{ } ^9\text{Be/g}$, Merchel et al., 2008). Target preparation involved adding
195 Nb (six times of the dry oxide weight). AMS measurements were conducted at DREAMS (DREs-
den AMS, Helmholtz-Zentrum Dresden-Rossendorf, 6 MV, Cu cathode) using the in-house standard
SMD-Be-12 (Akhmadaliev et al., 2013) normalized against the NIST SRM 4325 standard ($^{10}\text{Be}/^9\text{Be}$
ratio of $(2.79 \pm 0.03) \times 10^{-11}$, Nishiizumi et al., 2007). A round-robin exercise of AMS facilities
confirmed robust standard calibration and measurement configuration (Merchel et al., 2012). Pro-
200 cessing blanks were treated and measured parallel to the sediment samples. The blank isotope ratios
in the order of 0.3 - 1.7% ($^{10}\text{Be}/^9\text{Be}$ ratio of 2.0×10^{-15} and 2.1×10^{-15}) were subtracted from the
measured ratios of all samples.

3.4 Production rates and shielding factor

Representative ^{10}Be production rates and shielding were calculated by scaling the reference sea
205 level and high latitude (SLHL) production rate of 4.5 at/g quartz/yr (cf. Balco et al. 2008 according
to (Stone, 2000) to the conditions at individual sample basins (for details see the supplementary
material).

Accounting for the hypsometry of the whole basin involved ASTER GDEM (30 m resolution, NASA Land Processes Distributed Active Archive Center) processing to identify the upstream area
210 for each sampling site and calculate raster-cell resolved production rates and shielding. Assuming total shielding by permanent ice and snow cover, the production of ^{10}Be will only take place in areas that are actually exposed to the cosmic ray flux. To get representative rates, we excluded snow and ice covered areas from calculations of ^{10}Be production rates. The areas of permanent snow and ice cover are based on MODIS (Moderate Resolution Imaging Spectrometer) Land Cover
215 Type data MCD12Q1 (Strahler et al., 1999) and the classification scheme according to the IGBP (International Geosphere Biosphere Programm). The available data covers the years 2000 - 2012. For our calculations, we use the year 2010 that is among those with most extensive snow and ice cover. Variations in permanent snow and ice cover during the last millennia is unknown. Paleo-records only give information on glacier extents and do not include the distribution of snow cover nor does
220 MODIS data differ between snow and ice. We assume snow and ice cover to already have largely retreated since the last glacial maximum corresponding to the overall trend of retreating glaciers (e.g., Zech et al., 2005; Abramowski et al., 2006; Röhringer et al., 2012) that is also reported at historical time scales within the last roughly 50 years (Aizen, 2011; Gardelle et al., 2013). The area upstream of the Lake Yashilkul was not included into basin analyses as a large landslide dams the
225 plateau discharge and sediment flux. The dam is assumed to have been in place for several 10^4 years (Zech et al., 2005; Brookfield, 2008).

We estimated topographic shielding for each GDEM raster cell based on the horizon line within a 10 km distance according to the method of Codilean (2006). Norton and Vanacker (2009) found only low underestimation of shielding when using a DEM of 30 m resolution in steep terrain. Other
230 sources are considered negligible as snow and ice covered areas are already excluded from production rate calculation and vegetation is scarce due to the dry climate and high basin altitudes.

The raster-cell resolved production rates and shielding factors of each sampled basin show non-normal, skewed to poly-modal distributions due to topographic variations. We use the arithmetic mean to represent the conditions within the basins. Uncertainties are calculated based on the standard
235 variation to describe to the high value variability within basins. The uncertainties of denudation rates refer to the sum of errors from AMS measurements of the ^{10}Be concentration, and the variation of production rates and shielding.

3.5 Sample basin parameters

Basin-wide denudation rates have been found to correlate with altitude, slope, relief, precipitation or
240 glaciated area (e.g. Schaller et al., 2001; Montgomery and Brandon, 2002; von Blanckenburg, 2005; Norton et al., 2010). We describe the sampled basins in Pamir by probability density estimates of altitude, slope and precipitation (TRMM product 3B42 V7) using the R programming environment (R Core Team, 2013). We examine the influence of snow and ice covered areas on denudation rates

using the MODIS data of the year 2010 (see above) and calculating the covered area proportional to
245 the basin size. We characterize the relief of each sample basin using the altitude range at different
scales. The basin relief describes the overall range of altitudes by the difference between the 0.75
and 0.25 quartiles of basin altitudes. The use of quartiles compensates for the bias towards highest
relief for largest basins. The local relief represents the altitude range normalized to a given area. We
use a moving window of 1 km and 4 km width to analyze the GDEM data and determine the relation
250 between relief and denudation at the sub-basin scale. A smaller window size narrows relief estimates
down to slope, a wider window size reproduces trends of basin relief.

The median, 0.25 and 0.75 quartiles of each parameter serve for (multiple-) linear regression anal-
yses. This intends to discriminate the potential climatic and geometric parameters that can explain
the variance in denudation. The use of quartiles tests the relevance of the general condition within a
255 basin and evaluates the influence of low or high values of individual parameters. Linear regression
analyses is a standard tool for a simple, straightforward evaluation of basin characteristics. *Sensu*
stricto, correlation analyses based on linear regression are designed for normally distributed data.
We used the robust linear regression model available in the R environment (R Core Team, 2013) to
account for the small data set and reduce effects from any extreme values that skew the data. We
260 employ the coefficient of determination (R^2) as a quantitative indicator for basin parameters that
likely explain the variance of denudation rates and to be able to compare results to relations found in
other mountain regions. We do not rank the variables. The regression is meant to test which of relief
descriptors or climatic indicators describe better the variable denudation rate.

4 Results

265 4.1 Sample basin properties

The Panj river network is strongly asymmetric with the trunk reach connecting tributary outlets from
south to north close to the western drainage divide. The basins of the southern Panj and of the major
Panj tributaries show preferential east-west lengthened shapes (Fig. 1B). The parallel configuration
of the major basins allows to resolve south-north changes in factors controlling denudation. The
270 lengthened basins of the Gunt and Bartang Rivers (TA31B and TA01C) integrate over gradients
from the Pamir Plateau to its western margin. Here, the Shakh dara (TA30P) and Murghab Rivers
(TA08N) enable to discriminate the conditions in upstream areas related to the Pamir Plateau, while
the Vanj River basin (TA02A) has not plateau-related basin portions and represents solely marginal
conditions.

275 The median basin altitudes slightly decrease from 4800 to 4200 m a.s.l. along the course of the
Panj (cf. Fig. 1). The minimum altitudes representing the river bed markedly drop from 3600 to
700 m a.s.l. (Tab. 1) and reveal the downstream (northward) increase in the total altitude range with

increasing basin size. The strong decrease of minimum altitudes witnesses strong incision at the Pamir margins.

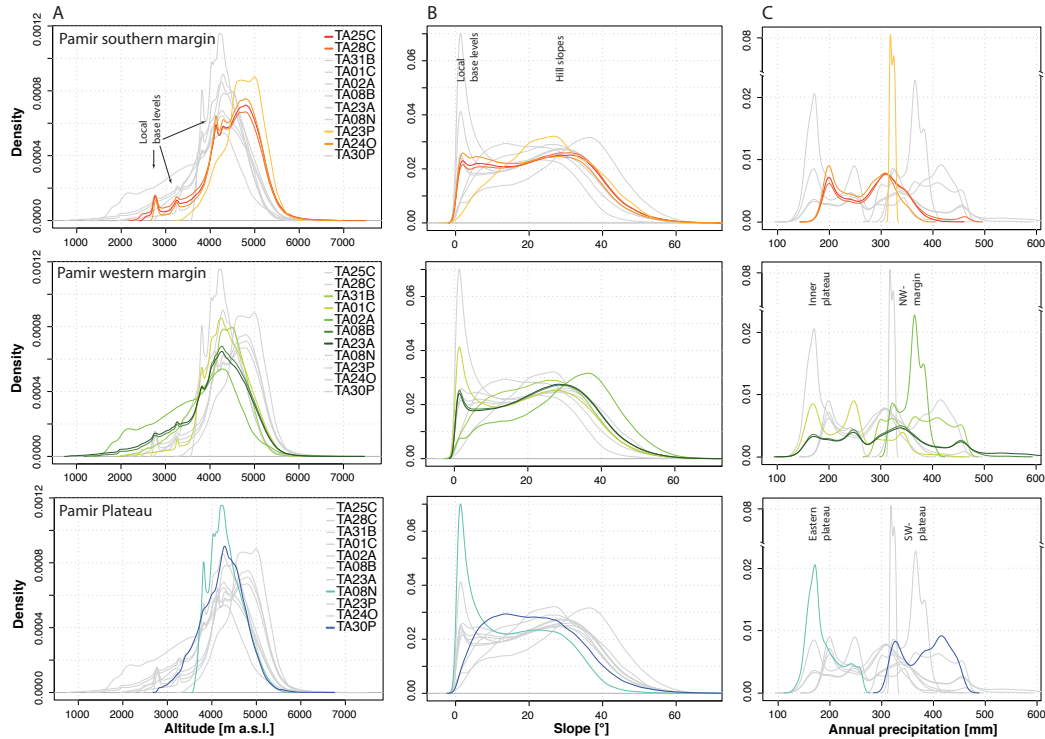


Figure 2. Frequency distributions of altitude (A), slope (B) and precipitation (C) for individual sample basins grouped due to their location at the southern or western margin of Pamir or at the Pamir Plateau. Relative frequencies of altitude and slope were calculated from a ASTER GDEM of 30 m resolution and precipitation from the TRMM product 3B42 V7 (Huffman et al., 1997, 2007) (notation of basins refers to bold fonts used for sample names in Fig. 1 and Tab. 1).

280 On the plateau, altitudes cluster between 3800 m a.s.l. and 5000 m a.s.l. with significantly less frequent lower altitudes (Fig. 2A, bottom). The basins of the southern Panj are slightly higher compared to those at the western Pamir margin. A strong drop in altitude frequencies delineates the Pamir Plateau from its margins (Fig. 2A). The main frequency contrast occurs at ~ 3800 m a.s.l. at the southern Pamir margin and less sharply at ~ 3600 m a.s.l. at the the western margin. Two minor peaks at ~ 3300 m a.s.l. and ~ 2800 m a.s.l. indicate local base levels below the Pamir Plateau
 285 (cf. Fig. 2A, top) in the southern Panj basins. The local base levels are masked in western Pamir basins by the increasing basin size. The Vanj basin (TA02A) stands out by its high proportion of margin-related altitudes indicating low influence from plateau-related areas.

The relative proportions of slopes within basins correspond to respective altitude distributions.
 290 Highly variable slopes display strongly bimodal distributions in the east-west elongated basins that

Table 1. Details on sampling sites and related upstream drainage area (sample basin). Ice: Permanent ice and snow cover based on the year 2010 from MODIS MCD12Q1 (Strahler et al., 1999), the given uncertainty represents the standard deviation of MODIS MCD12Q1 between 1998 and 2012. Altitude, slope and precipitation represent the median of the value distribution within sampled basins (see Fig. 2) calculated from the ASTER GDEM (30 m resolution). The rainfall data reflects the annual mean precipitation based on the Tropical Rainfall Measuring Mission (TRMM) product 3B42 V7, 1998-2012 (Huffman et al., 1997, 2007). Bold letters in sample names indicate notations used in the text and figures.

Sample	River	Location			Sample basin				
		Lon [°E]	Lat [°N]	Altitude [m a.s.l.]	Area [km ²]	Ice [%]	Altitude [m a.s.l.]	Slope [°]	TRMM [mm/yr]
<i>Panj:</i>									
TA090923A	Panj	70.177	37.901	731	71727	16.3 ± 2.9	4213	24.3	316
TA090908B	Panj	70.787	38.456	1220	67749	17.1 ± 3.0	4255	24.1	309
<i>Vanj:</i>									
TA090902A	Vanj	71.378	38.293	1551	2079	37.0 ± 6.5	3869	31.4	364
<i>Bartang:</i>									
TA090901C	Bartang	71.610	37.490	2030	29243	13.6 ± 2.4	4351	21.4	239
TA110808N	Aksu	73.965	38.161	3603	13548	4.0 ± 0.7	4283	14.5	176
<i>Gunt:</i>									
TA090831B	Gunt	71.527	37.490	2078	8437	18.7 ± 3.3	4294	23.3	376
TA110830P	Shakhdara	71.845	37.210	2785	3507	13.5 ± 2.4	4281	20.8	390
<i>southern Panj:</i>									
TA090828C	Panj	71.460	37.220	2275	15230	26.1 ± 4.6	4519	23.8	298
TA090825C	Panj	71.596	36.730	2491	13625	28.2 ± 4.9	4574	23.2	290
TA110824O	Panj	72.206	36.929	2754	11064	29.2 ± 5.1	4591	21.6	272
TA110823P	(Pamir)	72.737	37.173	3552	84	55.1 ± 9.6	4770	25.6	321

range over plateau and marginal basin portions (Fig. 2B, middle). The narrow peak of slope frequencies below 5° scales with the plateau-related, very flat basin portions between 4000 m and 5000 m a.s.l. (cf. upper Bartang, TA08N, Fig. 2B, bottom). Such areas are less extensive in the southern Panj basins that contour the Pamir at its southern margin Fig. 2B, top). The second, much broader frequency peak indicates hillslopes to cluster at roughly 35°. The Vanj basin (TA02A, Fig. 2, center) stands out with a negatively skewed slope distribution and maximum frequencies at ~40°. Although draining the Plateau, the Shakhdara basin (TA30P, Fig. 2B, bottom) displays a broad slope distribution with a plateau of high frequencies between 10° and 30° that suggests a transient position of the basin located on the edge of Pamir Plateau.

300 Areas of permanent ice and snow cover reflect the predominant moisture supply from the north-west and south, and evidence the aridity of the central-eastern parts of Pamir (Fig. 1B). The Pamir basins are very heterogeneously affected by ice and snow. The largest coverage of permanent ice and snow cover show the small basin of an upper Panj (Pamir River) tributary (TA23P, 55%) and the northernmost basin of the Vanj River (TA02A, 37%). In contrast, only 5% of the upper Bartang

305 (TA08N) basin at the eastern plateau are permanently covered by snow and ice (Tab. 1). A similar picture can be drawn from the median of TRMM-based mean annual precipitation (1998 - 2012). The largest basins TA23A and TA08B indicate an regional average of ~ 300 mm/yr. Variations in precipitation are mainly controlled by orographic gradients of the predominant atmospheric circulations.

310 **4.2 Denudation rate parameters**

The ^{10}Be concentrations show a high variability between sample basins (Tab. 2). Nuclide concentrations are comparable ($5.7 - 7.6 \times 10^4$ at/g) along the Panj and do not show any trend from upstream, smaller basins towards downstream basins of largest size. The tributary basins display a northward decrease in concentrations (TA31B, TA01C, TA02A) but the east-west elongated basins cause averaging of plateau-related and marginal basin portions. Especially concentrations measured for the Bartang basin (TA01C) is affected by including the upstream basin (TA08N) of highest ^{10}Be concentrations of $(98.5 \pm 2.1) \times 10^4$ at/g, while the downstream basin portion can be assumed to contribute very low concentrations to the sediment mix. Similarly, the Gunt basin (TA31B) comprises also the conditions in the Shakh dara River sub-basin (TA30P) that has two times the concentration found in the entire Gunt basin. The Vanj basin (TA02A) yields the lowest concentration with $(1.9 \pm 0.1) \times 10^4$ at/g.

Estimated production rates of ^{10}Be (cf. ^{10}Be production rates due to neutrons in Fig.1 of the supplementary material, top) correspond to the basin topography with one prominent maximum at ~ 80 at/g/yr. The increased altitude range at the western Pamir margin causes skewed distributions. Topographic shielding factors range from roughly 0.8 to 1.0 with a narrow and a wide maximum in frequencies (Fig. 1 in supplementary material, bottom) that mimic the distribution of slopes angles. Excluding areas covered by snow and ice lowers production rates in systematic manner, modulated by the amount of precipitation (Fig. 2 in supplementary material, A). Not excluding the ice and snow covered areas would result in erroneously high production rates because this includes among the highest basin portions where no ^{10}Be is produced. Such higher production rates would suggest a shorter time span for the acquisition of the measured nuclide concentration in the sediment. Excluding snow and ice covered areas reduces production rates that represent the areas exposed to the cosmic ray flux (Fig. 2 in supplementary material, A). The limited snow and ice coverage at the eastern plateau affects production rates less compared to those in the northwestern marginal basins. The effect on denudation rates amounts to less than 10% for all sample basins except TA23P and TA02A with up to 20% lower values. See the supplementary material for details on the parameters for denudation rate calculation including snow and ice covered areas, shielding corrected production rate.

Table 2. Parameters and results of denudation rate calculation. AMS measurements were performed at DREAMS, Helmholtz-Zentrum Dresden-Rossendorf. The ^{10}Be concentrations are corrected for processing blanks ($^{10}\text{Be}/^9\text{Be}$ ratios of 2.0×10^{-15} and 2.1×10^{-15} , i.e. 0.3-1.7% of the sample values). The effective production rate represents the sum of the neutron- and muon- (fast and stopped muons) induced production of ^{10}Be in quartz (P_{sum}), calculated using the scaling system of Stone (2000), and corrected for topographic shielding using the method of Codilean (2006). The values for individual basins are based on the arithmetic mean. T_{ave} gives the average time needed to erode the typical attenuation depth of ~ 60 cm as a proxy of ‘cosmogenic memory’, describing the time over which the cosmogenic nuclide inventory averages. Bold letters in sample names indicate notations used in the text and figures.

Sample	AMS	Production rate		Denudation rate	T_{ave}
	^{10}Be conc. [$\times 10^4$ at/g]	P_{sum} [at/g/yr]	Shielding [factor]	[mm/yr]	
<i>Panj:</i>					
TA090923A	5.7 ± 0.2	70.5 ± 17.3	0.92 ± 0.06	0.68 ± 0.23	880
TA090908B	6.7 ± 0.2	72.4 ± 17.3	0.92 ± 0.06	0.59 ± 0.20	1010
<i>Vanj:</i>					
TA090902A	1.9 ± 0.1	52.0 ± 13.3	0.87 ± 0.06	1.45 ± 0.56	410
<i>Bartang:</i>					
TA090901C	5.3 ± 0.2	79.5 ± 12.8	0.93 ± 0.06	0.83 ± 0.22	720
TA110808N	98.5 ± 2.1	80.2 ± 11.0	0.95 ± 0.04	0.05 ± 0.01	13010
<i>Gunt:</i>					
TA090831B	11.1 ± 0.4	73.1 ± 13.6	0.92 ± 0.06	0.37 ± 0.11	1640
TA110830P	25.5 ± 1.5	75.4 ± 12.0	0.93 ± 0.06	0.16 ± 0.05	3650
<i>southern Panj:</i>					
TA090828C	5.9 ± 0.3	78.3 ± 16.5	0.92 ± 0.06	0.74 ± 0.24	810
TA090825C	7.6 ± 0.3	80.4 ± 16.4	0.92 ± 0.06	0.58 ± 0.18	1030
TA110824O	6.3 ± 0.6	81.7 ± 14.2	0.93 ± 0.06	0.72 ± 0.24	830
TA110823P	5.7 ± 0.2	84.7 ± 11.1	0.89 ± 0.06	0.79 ± 0.19	760

4.3 Basin-wide denudation rates

340 Resulting rates of the two largest basins (TA23A and TA08B) reveal an high average denudation for
the entire Pamir with ~ 0.64 mm/yr (Fig. 3). Denudation rates determined along the Panj resemble
the average conditions and stay relatively consistent despite significant changes in basin sizes. Mi-
nor variations indicate a slight, westward decrease in denudation with increasing size of the south-
ern Panj basins. The denudation rate of (0.79 ± 0.19) mm/yr for the eastern, upper Panj (TA23P,
345 small Pamir River tributary) lowers to (0.58 ± 0.18) mm/yr for the entire southern Panj basin be-
fore the river course deflects to the north. The denudation rates rapidly increases downstream to
 (0.74 ± 0.24) mm/yr despite a relatively modest increase of drainage ($\sim 13\%$).

The rates of the major Panj tributaries (Gunt, Bartang, Vanj) reveal strong contrasts in denudation across the Pamir ranging from (0.05 ± 0.01) mm/yr to (1.45 ± 0.56) mm/yr (Tab. 2). The pattern of denudation illustrates increasing rates from the south-eastern central plateau towards the north-western margins. Two upstream sub-basins determine low denudation on the Pamir Plateau with (0.05 ± 0.01) mm/yr for the easternmost inner plateau (TA08N) and (0.16 ± 0.05) mm/yr for the south-western Shakhhdara basin (TA30P). The morphometry of those plateau-related areas is characterized by the predominance of altitudes above 3600 m a.s.l. and large areas of slopes below 5° (cf. Tab. 2). Denudation rates determined immediately before the confluence with the Panj show a northward increase from ~ 0.37 mm/yr to 1.45 mm/yr in major tributary basins (Gunt, Bartang, Vanj). Rates of the elongated Gunt (TA31B) and Bartang (TA01C) basins integrate the low denudation of upstream plateau-related sub-basins (TA08N and TA30P). Consequently, denudation in downstream basin portions across the Pamir margin lies above the basin-wide average. The differentiation of high denudation in marginal sub-basins fits to the denudation rate of (1.45 ± 0.56) mm/yr for the Vanj basin (TA02A) that reflects conditions at the northwestern Pamir margin without significant portions of the typically flat, plateau-related basins.

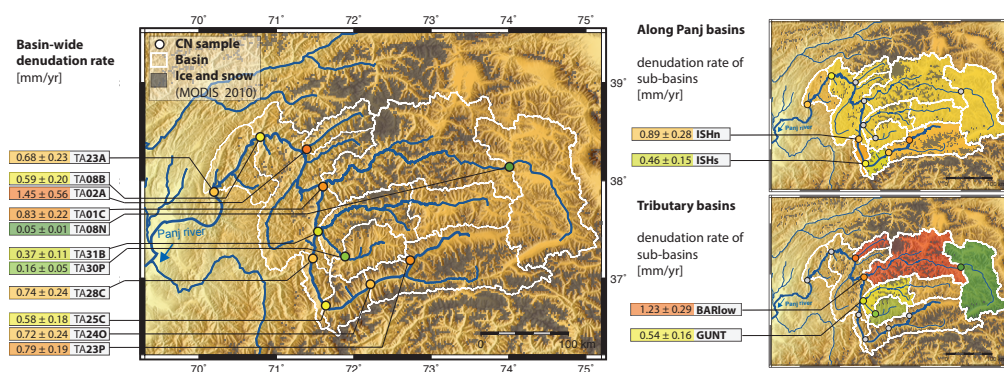


Figure 3. Basin-wide denudation rates of along Panj and major tributary samples (CN: cosmogenic nuclide, color code represents magnitude of denudation with green for low and red for high rates). Calculations base upon AMS measurements of ^{10}Be concentrations in modern fluvial sediments and GDEM processing for production rates and topographic shielding. Denudation rates of the sub-basins ISHn, ISHs, BARlow and GUNT represent slope weighted estimates inferred from sampled basins (respective *up* and *down*-stream basins) and using derived measurement results in equation 3 (for details see text and Tab. 3).

We estimate the denudation rates of the lower portions of the Gunt (GUNT) and the Bartang (BARlow) by relating rates of the upstream basin area for which we have data to those of the entire basins. We scaled the denudation rates by their relative area as a simple approximation. The average

Table 3. Approximated denudation rates of sub-basins using weighting factors that account for basin area (a) and basin slope (s). The weighting factors a and s are applied to determine variations in denudation within large basins when the rates are known (determined based on measured ^{10}Be concentrations and respective production rates) for the entire basin and one of its sub-basins (ε : denudation rate, total: sample data for entire basin, up: sample data for upper sub-basin, down: inferred rate for lower sub-basin using the *area* or *slope*-based weighting factors, a : area factor describing the proportion of the respective sub-basin normalized to 1, s : slope factor describing the slope variations of sub-basins normalized to 1).

Basin	Denudation rate [mm/yr]				Basin area		Basin slope	
	ε_{total}	ε_{up}	$\varepsilon_{down(area)}$	$\varepsilon_{down(slope)}$	a_{up}	a_{down}	s_{up}	s_{down}
Gunt	0.37 ± 0.11	0.16 ± 0.05	0.53 ± 0.16	0.54 ± 0.16	0.44	0.56	0.45	0.55
Bartang	0.83 ± 0.22	0.05 ± 0.01	1.64 ± 0.38	1.23 ± 0.29	0.51	0.49	0.34	0.66
Southern Panj (TA25C)	0.58 ± 0.18	0.72 ± 0.24	0.02 ± 0.01	0.46 ± 0.15	0.80	0.20	0.47	0.53
Southern Panj (TA28C)	0.74 ± 0.24	0.58 ± 0.18	1.81 ± 0.57	0.89 ± 0.28	0.87	0.13	0.49	0.51

denudation rate for the entire basin (ε_{total}) represents the sum of area-weighted denudation rates in its upper and lower sub-basins (*up* and *down*) by

$$\varepsilon_{total} = a * \varepsilon_{up} + (1 - a) * \varepsilon_{down} \quad (3)$$

The area factor a (normalized to 1) describes the portion of the upstream sub-basin relative to the area of the entire basin. The approach yields area-weighted denudation rates of 0.53 mm/yr (GUNT) and 1.64 mm/yr (BARlow) for downstream basin portions (ε_{down} , Tab. 3). Applying the same approach to the southern Panj basins enhances the contrast in denudation where the southern Panj deflects to the north at the western Pamir margin. The relative areas of the basin TA24O and TA25C indicate an denudation rate of only 0.02 mm/yr for the inferred sub-basin ISHs. In contrast, the inferred sub-basin between TA25C and TA28C (ISHn) suggests a very high denudation rate of 1.81 mm/yr, comparable to those of the lower Bartang basin (BARlow) and the Vanj basin (TA02A). However, the area-weighted denudation rates may be biased as the actual contribution of individual basin portions to the sampled mix of material remains unresolved.

The area factor a can be replaced by a slope factor s to account for morphometric differences in basin portions. The factor s describes the ratio of the sub-basin slope scaled to the slope of the entire basin and normalized to 1 (i.e. division by 2 in the case of two basins). Slope-weighted denudation rates are then determined by using the equation 3. Inferred rates indicate an improved fit to morphometric units and respective trends in basin-wide rates of measurement data. The slope-weighted denudation rates are 0.54 mm/yr for the sub-basin GUNT, 1.23 mm/yr for BARlow, 0.46 mm/yr for ISHs and 0.89 mm/yr for ISHn (Tab. 3).

4.4 Relationship between denudation rates and basin parameters

The absence of any trend with increasing basin size suggests no significant nuclide acquisition during grain transit through the basin. Results reveal a primary role of topographic basin parameters on variations of denudation rates (Fig. 4). The basin-wide denudation rates indicate a relationship to measures of the altitude range within basins, but the goodness of this relation strongly depends on scale, i.e. the reference area used to quantify the range of altitudes. The basin relief (BR, Fig. 4A) is not suited to explain rates of denudation, while the local relief (LR, Fig. 4A) yields an R^2 of 0.68, when being estimated within 1 km. The highest correlation to denudation rates is attained with basin slope gradients. Using the median slopes yields an R^2 of 0.73. The steep slopes of a basin seem to be even more important as the 0.75 quartiles of basin slopes explain denudation rates with an R^2 of 0.81 (Fig. 4B). The correlation of denudation with slopes suggests that the slope-weighted denudation rates for the inferred sub-basins GUNT, BARlow, ISHs and ISHn suite the primary relationship found in regression analyses (Tab. 3).

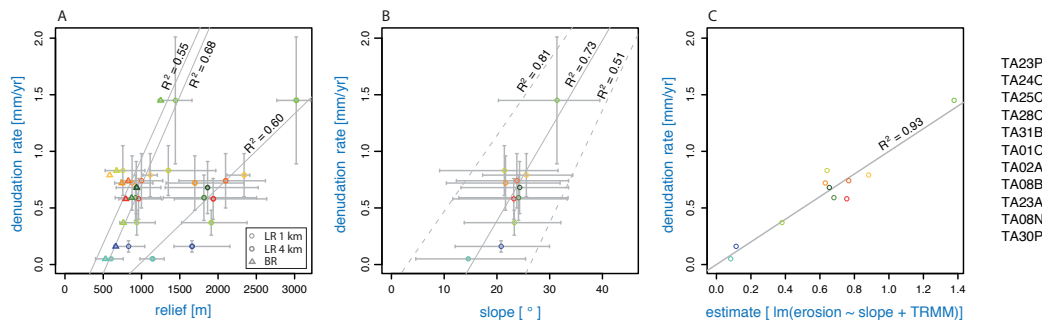


Figure 4. Robust linear regression analyses for denudation rates and the basin parameters relief (A), slope (B) and slope combined with precipitation (C). A: Scale-dependent relief calculation (BR: Basin relief representing the difference between the 0.75 and 0.25 quartiles of basin altitudes, LR: Local relief determining the altitude range within a moving window of 1 km and 4 km, respectively. Values of each basin represent the median and the range between the 0.75 and 0.25 quartiles). B: Basin slopes representing the median of slopes within individual basins. Slope variations are shown according to the 0.25 and 0.75 quartiles. C: Multiple linear regression revealed highest correlation of denudation rates with the 0.75 quartiles of basin slope and TRMM-based precipitation (lm: linear model used for multiple linear regression analyses). Solid lines show the robust linear regression for median values, dashed lines that of respective quartiles. R^2 gives the coefficient of determination.

The only slight variations in mean annual rainfall between 270 mm and 380 mm (based on TRMM rainfall data) cannot explain the pattern of denudation (R^2 of < 0.1). Similar denudation rates cluster regardless of relatively lower or higher precipitation, while highest denudation relates to basins receiving highest annual precipitation. The limited influence of precipitation on denudation may relate to the overall low precipitation, predominantly in form of snow and temperature induced peak

discharge in the melting season. The relative area covered by snow and ice shows no strong relation
405 to denudation rates with an R^2 of < 0.4 .

We performed a multiple linear regression analysis with two components as predictors for denudation to test for additive effects of basin properties. Other regression models are possible but inappropriate for the small data set and less comparable to any linear relations found for the one predictor linear regression performed at first. The multiple linear regression addresses the question
410 if any predictor requires preconditions to become effective. Including more components resulted in multi-collinearity and insignificant effects on the goodness of correlation. The best results were obtained by combining the 0.75 quartiles of slope and TRMM data with a R^2 of 0.93 (Fig. 4C) suggesting a good fit of the additive linear model. Other two predictor combinations yielded lower R^2 values than the linear regression using only slope angles as predictor of the denudation rates. The
415 regression with slope gradient and TRMM rainfall data indicates that low slopes imply low denudation despite variations in precipitation, while high precipitation contributes to high denudation rates in the case of steep slopes. All other parameter combinations yielded lower correlations.

5 Discussion

5.1 Averaging times of Pamir denudation rates

420 For a robust interpretation of the Pamir denudation rates, it is important to consider the scales of averaging in terms of time and space. The denudation rates in Pamir average over time scales of 10^2 to 10^4 years i.e. the Holocene (Tab. 2). The high denudation rates for most of the Pamir basins imply a T_{ave} of less than 10^3 years. Such short time intervals for the renewal of the nuclide inventory suggest that the denudation rates represent modern conditions. Although the climate likely
425 underwent fluctuations, there is no evidence for major changes during that time in glacial records (Zech et al., 2005; Abramowski et al., 2006; Röhringer et al., 2012). The moderate denudation rates (about 0.16-0.37 mm/yr) calculated for the Gunt (TA31B) and the Shakh dara basins (TA30P) average over the time since the middle/late Holocene. Only the eastern Pamir Plateau basin (TA08N) has a significantly longer T_{ave} averaging denudation over the time since the MIS 2 - MIS 1 transition (Tab. 2). This integrates over the Holocene deglaciation period but the large areas of low
430 slopes formed by sediment-filled valleys of the inner Pamir are indicative of low denudation persistent over long time scales. Additionally, influences of short-term environmental fluctuations on denudation rates decreases with increasing nuclide concentration and averaging time, respectively. However, the estimated T_{ave} means that variations in the absolute extent of glaciated areas are possible. T_{ave} is largely longer than the period covered by available MODIS data on permanent snow
435 and ice (MCD12Q1, Strahler et al., 1999, year 2010) distribution and mostly too short to be resolved by glacial chronologies at the Pamir Plateau. We assume persistent climatic circulations and dry

conditions during the last 10^2 yr to 10^3 yr with only slightly more extensive coverage of snow and ice compared to our chosen reference, the MODIS data of the year 2010.

440 Another point to consider in terms of time scales is the nuclide built-up during grain transport from the source rock to the sampled site. Robust cosmogenic nuclide-derived denudation rates require that grain travel time through the sampled basin should be short compared to T_{ave} (Granger et al., 1996; von Blanckenburg, 2005; Dunai, 2010). A significant nuclide built-up would result in a downstream increase of ^{10}Be concentrations (Schaller et al., 2001), but such increasing nuclide
445 concentrations are not indicated for sampled basins along the Panj. Concentrated discharge during the melting season and also the generally high slope angles (0.75 quartiles of 25 - 40°), especially in marginal downstream basin portions, may be responsible for the annual sediment transported over long distances. Only valleys in the plateau-related basins contain significant sediment fills and witness relatively long storage periods. Nevertheless, this is in agreement with determined denudation
450 rates.

Centennial to millennial scale ^{10}Be -based denudation rates in tectonically active landscapes such as the Pamir can be dependent on the magnitude-frequency distribution of mass wasting (e.g., Wolman and Miller, 1960; Korup et al., 2010; Korup, 2012; Lupker et al., 2012). High-magnitude events deliver sediments to river channels at a low frequency, but their effects on the sediment yield of a
455 basin may be captured with increasing time intervals at decadal scale or longer (Wolman and Miller, 1960; Korup, 2012). The low abundance of such events in the study area (e.g. Lake Yashilkul upstream of the Gunt River) indicates their minor relevance.

On the 10^6 year time scale, Stübner et al. (2013) estimated syn- to post-tectonic erosion rates of 0.3 - 0.5 mm/yr for the southern Pamir Shakh dara Dome and 0.1 - 0.3 mm/yr between the Shakh dara
460 and Alichur Dome based on geometric constraints. These long-term estimates agree to the cosmogenic nuclide-based denudation rates of the same area. The higher rates fit to the marginal conditions of the Gunt basin, while the lower rates agree to conditions related to the inner southern Pamir (Shakh dara basin). The indication of persistent low erosion over time scales of 10^4 to 10^6 suggests a long-term steady-state on the plateau of Pamir. The higher rates of ~ 0.7 mm/yr and up to ~ 1.5
465 mm/yr in most other basins at the Pamir margins delineate areas undergoing adjustment to uplift or base level drop at millennia scale. The high rates roughly compare to the up to 2.0 mm/yr of erosion inferred by Carrapa et al. (2014), who associate the intense erosion to persistent feedbacks between exhumation and pronounced precipitation in the western Pamir. Erosion rates from river load gauging are not available yet, but may greatly differ from the ^{10}Be -based rates as they enable
470 to resolve (below) decadal variations at smaller scales and are more dependent on the frequency of high-magnitude events and hillslope-river channel connectivity.

5.2 Spatial variations in denudation rates

The basin-wide denudation rates represent average values for their upstream areas. They may be biased in tectonic active landscapes when certain basin portions deliver unproportional high amounts of sediments to the river channels, for example in form of landslides (e.g. Granger et al., 1996; von Blanckenburg, 2005; Dunai, 2010). For our samples, most basins are large enough to average effects of single basin portions. Besides, they also average over differences in the erodibility and quartz abundance of rock types. However, the sediment release from individual geomorphic units within sample basins is certainly not uniform. Hence, small scale in situ data are needed to resolve the erosional domains within the studied basins and refine individual sediment contributions to the river channels.

In particular, the sediment delivery from snow and ice covered areas requires attention. There is currently no ideal way to deal with such totally shielded areas of a basin. We excluded respective areas based on the permanent snow and ice cover (MODIS MCD12Q1, Strahler et al., 1999, year 2010) to derive production rates representative of basin portions exposed to the cosmic ray flux, where ^{10}Be is actually produced in situ in quartz grains. However, the snow and ice covered areas contribute sediments that likely were completely shielded before (glacio-)fluvial transport and hence, bear negligible ^{10}Be concentrations that do not scale with the rate of denudation. Calculating denudation rates from such diluted ^{10}Be concentrations using production rates from the non-snow and ice areas of a basin (Fig. 4A) has several consequences. The excluded areas comprise the highest altitude of a basin and exclusion lowers the production rates on the basin scale. But this does not necessarily scale with the amount of sediment exported this snow and ice covered areas and may be insufficient especially in the case of large quantities of glacial sediments in the sampled material. Grains exported by glacio-fluvial transport dilute the CN concentration with zero-CN-grains that mimic instant erosion independent of the actual rate below the glacier. The effect on the total basin-wide denudation rate depends on the efficiency of glaciers to erode. But exactly the efficiency of glacial processes on denudation is highly debated (Norton et al., 2010; Godard et al., 2012, e.g.). The portion of grain exported from the excluded snow and ice covered areas is still unknown for the sampled basins. Further small-scale data of sediment yields may resolve the influence of glaciated and non-glaciated areas and that of snow covered areas within basins on the absolute magnitudes and variation of denudation rates for the major basins of the Pamir. Nonetheless, analyses of sediment yields on an annual basis do not indicate a significant relationship with meteorological factors such as temperature and glaciated areas (Pohl E., and Gloaguen R., per. comm.). Remobilisation of sediments from moraines is possible, but such glacial deposits are older than the time span captured by our data and are mainly found at the Pamir Plateau, where denudation is minimal. Their contribution to river sediments indicates thus marginal influence. The influence of the relative abundance of glaciers within our studied basins seems non-systematical as we could not find a correlation between percentage of snow and ice coverage and denudation rates.

The average denudation rates of basins along the Panj outline an overall agreement with the Pamir
510 average of ~ 0.64 mm/yr without any clear trend from smaller to larger basins (Fig. 3). In contrast,
the studied tributaries reveal strong spatial variations in denudation. The major tributary basins in-
dicate increasing denudation to the northeast. The east-west elongation of the tributary basins cause
averaging across the plateau and its margins, while the Vanj basin (TA02A) is de-coupled from the
plateau. The slope-weighted calculation allows to account for the differing morphometries of the
515 lower and upper Gunt (TA31B and TA30P) and Bartang (TA01C and TA08N) basin portions that are
averaged in estimates for the entire basin. This approach supports the delineation of very low denuda-
tion (about 0.05 - 0.16 mm/yr) in plateau-related areas and higher rates (about 0.54 - 1.45 mm/yr) in
marginal (sub-)basins.

Overall, the ^{10}Be -based basin-wide denudation rates are 10 times lower than reported OSL-based
520 incision rates along the Panj. Those incision rates cover the last major deglaciation period, but indi-
cate persistent rates over the last 26 kyr, while variations in magnitude suggest a dominant control
from local factors (Fuchs et al., 2014). The discrepancy between the basin-wide denudation and flu-
vial incision rates indicates that the basin-wide denudation does not balance the lowering of the local
base levels induced by the intense fluvial incision of the Panj at the Pamir margins. Despite the dif-
525 ference in magnitude, the spatial pattern agrees between fluvial incision along the Panj river profile
and variations in denudation rates (Fig. 5). Denudation rates slightly decrease with the increasing
southern Panj basin (TA25C) to (0.58 ± 0.18) mm/yr and abruptly increase to (0.74 ± 0.24) mm/yr
where the Panj turns to the north cutting across the Shakh dara Dome (Fig. 5; Fuchs et al., 2013,
2014) and where intensified fluvial incision of 7 - 10 mm/yr drives base level lowering. The changes
530 in process rates correspond to other geometric measures such as valley shape ratios (VSR), Hack
Indices and riverbed convexity (Fig. 5). The slope-weighted estimates (ISHs and ISHn) enhance the
contrast in denudation by an increase from (0.46 ± 0.15) mm/yr to (0.89 ± 0.28) mm/yr and suggest
to represent the local morphometric conditions. Lower denudation rates of (0.37 ± 0.11) mm/yr for
the entire Gunt basin (TA31B) coincide with lower incision rates determined north of the confluence
535 with the Gunt River, where the Panj develops a more graded river profile (Fig. 5). Further north, av-
erage denudation rates of the Bartang (TA01C) and Vanj basins (TA02A) increase from 0.83 mm/yr
to 1.45 mm/yr. This trend is not resolved in OSL-based incision rates that vary between 4 mm/yr and
6 mm/yr and are, on the relative scale, better comparable to the Pamir-wide average denudation rates
of ~ 0.64 mm/yr. The de-coupling of the trends in denudation rates of northern tributary basins from
540 the incision may relate to the already large Panj basin that becomes less sensitive to signals recorded
by smaller tributary basins.

The magnitude of denudation is comparable with rates determined across the steep escarpment of
the Himalaya (e.g. Godard et al., 2010; Andermann et al., 2012; Burbank et al., 2012; Lupker et al.,
2012; Scherler et al., 2014), although conditions are different in Pamir. The monsoon-controlled
545 southern flank of the Himalaya receives precipitation of up to 4 m/yr, where erosion rates exceed

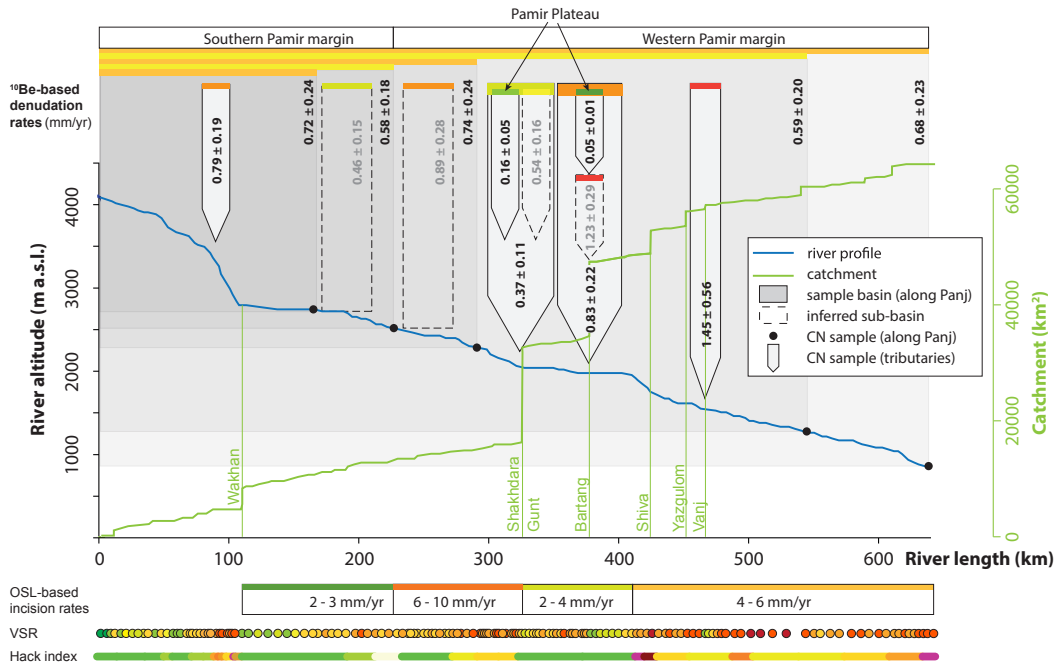


Figure 5. Variation of basin-averaged denudation rates and fluvial incision along the Panj (CN: cosmogenic nuclide, OSL: optically stimulated luminescence). The along Panj samples (filled circles) represent ^{10}Be -based denudation rates that integrate over related upstream areas (grey shaded areas). Major tributaries and their sub-basins show local differences in denudation between marginal and plateau-related basin portions. The color code illustrates the magnitude of denudation rates (green: low, red: high) and indicates the respective basin area. OSL-based incision rates, valley shape ratios (VSR) and Hack indices (Fuchs et al., 2013, 2014) along the Panj represent the pattern of fluvial incision that determines the lowering of local base levels at the Pamir margins.

2 mm/yr, while rates lower to ~ 0.1 mm/yr in the northern rain shadow of the Higher Himalayan and Tibetan Plateau (Burbank et al., 2012, e.g.). Gabet et al. (2008) correlated erosion based on sediment flux in Nepal rivers to average monsoon precipitation with an R^2 of ~ 0.9 . The sediment flux broadly scales with discharge. Suspended load data shows sediment flux dependent on the magnitude-frequency distribution of rainfall such that sediment pulses require an initial amount of precipitation (Andermann et al., 2012; Burbank et al., 2012). Andermann et al. (2012) emphasize the role of intense precipitation on generating direct runoff and sediment supply from hillslopes. The temperature-sensitive discharge in the high elevated northern rain shadow modulates the relation by peak discharge during the melting season. The hysteresis of sediment load and discharge suggests a supply limited behavior (Andermann et al., 2012; Burbank et al., 2012). Godard et al. (2014) describe a strong increase in denudation from 0.5 - 1 mm/yr in the Lesser Himalaya to 2 - 3 mm/yr in the Greater Himalaya despite relatively similar precipitation rates (R^2 of 0.13). They suggest denuda-

tion adapting fast to climatic changes and infer first-order control from large-scale tectonic uplift rates (R^2 of 0.78). The control of tectonic uplift on long-term erosion ($\sim 10^5$ years, based on thermo-
560 chronology) agrees in uniform rates across the Greater Himalaya despite a fivefold increase in precipitation (Burbank et al., 2003). A primary control of tectonic-driven topographic steepness on erosion suggests that changes in precipitation are balanced by complex interactions between channel steepness and width, and concentrated sediment transport (Burbank et al., 2003; Scherler et al., 2014).

565 Steep slopes are also the primary factor controlling denudation in Pamir (R^2 of 0.81) out of the sets of predictors that we looked at. Low denudation rates of < 0.2 mm/yr are linked to the high-elevated, low-relief inner-plateau areas that basically comprise the uplifted Cenozoic domes of the southern, central and eastern Pamir and wide, sediment filled valleys. At the Pamir margins, rapid base level lowering by the Panj facilitates steep slopes that in turn suggest high denudation rates. But the rates
570 of 0.54 - 1.45 mm/yr in marginal basin do not balance the intense fluvial incision. The discrepancy may relate to a possible fast base level drop cause by river captures across the Pamir domes (Fuchs et al., 2013, 2014), while hillslopes adjustment is limited. Highest rates coincide with increased precipitation at the north-western Pamir margin and suggest complex links between denudation, slopes angles and precipitation. Precipitation alone does not reveal any correlation to denudation
575 rates (R^2 of < 0.1). Combined with the parameter slope, multiple linear regression analyses suggests that both parameters can explain most of the denudation variance (R^2 of 0.93). This multiple relation indicates that steep slopes are the important precondition for precipitation to become a relevant driver of denudation. In the overall dry Pamir, our data suggests that precipitation is a limiting factor for high denudation rates. Basins of highest denudation receive precipitation mainly in winter in form
580 of snow that causes a temperature-sensitive concentration of discharge during the melting season. The seasonal peak discharge may be responsible for an efficient sediment flux out of basins that explains the lowest discrepancy between hillslope processes and fluvial incision in the north-eastern Pamir. The highest discrepancy between denudation and fluvial incision coincides with the southern Pamir margins, where less precipitation is available for sediment transport from hillslopes and out
585 of basins. Although rapid, fluvial incision induces persistent, steep slopes as the first order control, denudation rates indicate a precipitation-limited response.

6 Conclusions

The basin-wide denudation rates of ~ 0.64 mm/yr for the entire Pamir highlight a rapid landscape evolution. This regional-scale denudation averages over very different morphometric units of the orogen. Individual sub-basins of the major tributaries emphasize strong contrasts in denudation between
590 the Pamir margins (0.54 mm/yr to 1.45 mm/yr) and the inner plateau (0.05 mm/yr to 0.16 mm/yr). The pattern of denudation reveals fast material removal related to high variations in altitude and

local base levels at the margins, and much longer residence of material where large flat areas define the constant local base level of the Pamir Plateau.

595 Topography affects denudation rates in Pamir especially through the prevalence of steep slopes (0.75 quartiles) that explain about 80% of the variance in denudation (R^2 of 0.81). The persistence of steep slopes implies either tectonic uplift or base level lowering. The steep slopes drive fast material supply to the river channels. Maintaining the steep slopes and related sediment flux largely depends on the capacity of rivers to transport the sediment out of the basins. Consequently, this also could
600 indicate a climatic component affecting the river discharge.

Highest denudation rates at the Pamir margin coincide spatially with orographic precipitation delivered by the Westerlies, but our estimated denudation rates show no correlation to mean annual precipitation. The snow and ice coverage does not correlate (R^2 of <0.4) with denudation. Multiple linear regression analyses with an R^2 of 0.93 outlines that steep slopes are an important precondition
605 for the efficiency of denudation but also that a minimum of precipitation is required to allow the sediment transport in Pamir.

The water available for denudation shows high spatiotemporal variations (Pohl et al., 2014). It is largely controlled by the predominance of winter precipitation and its delayed release during the melting season. The resulting seasonal peak discharge during spring and early summer provides the
610 condition for an effective sediment mobilization out of basins (Pohl et al., 2014) and hence, favours high denudation especially at the north-western Pamir margin. The drier Pamir Plateau does not generate sufficient discharge which results in the prevalence of low slopes corresponding to low denudation rates.

The magnitude of denudation is similar to rates determined across the south Himalayan escarpment and Tibetan Plateau (e.g. Godard et al., 2010; Andermann et al., 2012; Burbank et al., 2012; Lupker et al., 2012; Scherler et al., 2014), although both climatic and tectonic conditions are different in Pamir (e.g. Fuchs et al., 2013). In the Himalayas, a much higher amount of summer precipitation allows that the landscape adjusts faster to uplift conditions and fluvial processes compensate for variations in precipitation (e.g., Burbank et al., 2012). In the much drier Pamir, this adjustment is
620 not reached. Incision clearly exceeds uplift. Basin-wide denudation rates do not balance the up to 10 times faster OSL-based incision rates measured along the Panj river (Fuchs et al., 2014). This significant discrepancy implies a transient landscape, for which precipitation is the limiting factor for hillslope adjustment to fluvial incision and for which we propose that river captures are responsible for the strong base level drop that drives incision along the Panj.

625 The limited coupling of denudation and incision has important implications on landscape evolution models and geohazard prediction (e.g., Gruber and Mergili, 2013). The dry conditions/low winter precipitation may limit the hillslope response to base level lowering to the close vicinity of the river channel itself, and hence, may intensify effects from hillslope length and channel network density. The strong incision and narrow wavelength of hillslope response suggest local relief steep-

630 ening with increasing risks of sudden slope failures and resulting debris flows or landslides. Additionally, the case of the Pamir shows not only the complex interplay of tectonic and climatic factors, but highlights especially the importance of internal feedbacks in an evolving drainage system, here in form of river captures, that require implementation in landscape models.

Acknowledgements. We would like to thank the Department of Meteorology and Hydrology of Tajikistan for the support and organization during fieldwork in 2011. We are also grateful for the support of the DREAMS operator team facilitating AMS beam time, with special thanks to Shavkat Akhmadaliev, Stefan Pavetich and René Ziegenrücker. And we thank the DFG for funding our research associated with the TIPAGE project (GI362/4-1). We used GMT (Wessel, P. and W. H. F. Smith, New, improved version of the Generic Mapping Tools released, EOS Trans. AGU, 79, 579, 1998), QGIS (<http://qgis.org/>) and the R environment (<http://www.r-project.org/>) for 640 most of the topographic data processing and the resulting figures. MODIS MCD12Q1 and ASTER GDEM data products were obtained through the online Data Pool at the NASA Land Processes Distributed Active Archive Center (LP DAAC), located at the U.S. Geological Survey (USGS) Earth Resources Observation and Science (EROS) Center, Sioux Falls, South Dakota (https://lpdaac.usgs.gov/data_access).

References

- 645 Abramowski, U., Bergau, A., Seebach, D., Zech, R., Glaser, B., Sosin, P., Kubik, P. W., and Zech, W.: Pleistocene glaciations of Central Asia: Results from ^{10}Be surface exposure ages of erratic boulders from the Pamir (Tajikistan), and the Alay–Turkestan range (Kyrgyzstan), *Quaternary Science Reviews*, 25, 1080–1096, 2006.
- Aizen, V.: Pamir glaciers, in: Sigh, V.P., Singh, P., Haritashya, U.K. (Eds.): *Encyclopedia of Snow, Ice and*
- 650 *Glaciers*, pp. 813–815, 2011.
- Akhmadaliev, S., Heller, R., Hanf, D., Rugel, G., and Merchel, S.: The new 6 MV AMS-facility DREAMS at Dresden, *Nuclear Inst. and Methods in Physics Research*, B, 294, 5–10, 2013.
- Andermann, C., Crave, A., Gloaguen, R., Davy, P., and Bonnet, S.: Connecting source and transport Suspended sediments in the Nepal Himalayas, *Earth and Planetary Science Letters*, 351–352, 158–170, 2012.
- 655 Balco, G., Stone, J. O., Lifton, N. A., and Dunai, T. J.: A complete and easily accessible means of calculating surface exposure ages or erosion rates from ^{10}Be and ^{26}Al measurements, *Quaternary Geochronology*, 3, 174–195, 2008.
- Bershaw, J., Garzzone, C. N., Schoenbohm, L., Gehrels, G., and Tao, L.: Cenozoic evolution of the Pamir plateau based on stratigraphy, zircon provenance, and stable isotopes of foreland basin sediments at Oytay
- 660 (Wuyitake) in the Tarim Basin (west China), *Journal of Asian Earth Sciences*, 44, 136–148, 2012.
- Bierman, P. R. and Steig, E. J.: Estimating rates of denudation using cosmogenic isotope abundances in sediment, *Earth Surface Processes and Landforms*, 21, 125–139, 1996.
- Bookhagen, B., Thiede, R. C., and Strecker, M. R.: Late Quaternary intensified monsoon phases control landscape evolution in the northwest Himalaya, *Geology*, 33, 149–152, 2005.
- 665 Brookfield, M. E.: Evolution of the great river systems of southern Asia during the Cenozoic India–Asia collision: Rivers draining north from the Pamir syntaxis, *Geomorphology*, 100, 296–311, 2008.
- Brown, E. T., Edmond, J. M., Raisbeck, G. M., Yiou, F., Kurz, M. D., and Brook, E. J.: Examination of surface exposure ages of Antarctic moraines using *in situ* produced ^{10}Be and ^{26}Al , *Geochimica et Cosmochimica Acta*, 55, 2269–2283, 1991.
- 670 Brown, E. T., Stallard, R. F., Larsen, M. C., Raisbeck, G. M., and Yiou, F.: Denudation rates determined from the accumulation of *in situ*-produced ^{10}Be in the Luquillo Experimental Forest, Puerto Rico, *Earth and Planetary Science Letters*, 129, 193–202, 1995.
- Burbank, D. W. and Anderson, R. S.: *Tectonic geomorphology*, Blackwell Science, Wiley, 2000.
- Burbank, D. W., Blythe, A. E., Putkonen, J., Pratt-Sitaula, B., Gabet, E., Oskin, M., Barros, A., and Ojha, T. P.:
- 675 *Decoupling of erosion and precipitation in the Himalayas*, *Nature*, 426, 652–655, 2003.
- Burbank, D. W., Bookhagen, B., Gabet, E. J., and Putkonen, J.: Modern climate and erosion in the Himalaya, *Comptes rendus - Geoscience*, 344, 610–626, 2012.
- Burtman, V. S. and Molnar, P.: Geological and physical evidence for deep subduction of continental crust beneath the Pamir, *GSA Special Papers*, 281, 1–76, 1993.
- 680 Carrapa, B., Shazanee Mustapha, F., Cosca, M., Gehrels, G., Schoenbohm, L. M., Sobel, E. R., DeCelles, P. G., Russell, J., and Goodman, P.: Multisystem dating of modern river detritus from Tajikistan and China: Implications for crustal evolution and exhumation of the Pamir, *Lithosphere*, 2014.

- Champagnac, J.-D., Schlunegger, F., Norton, K., von Blanckenburg, F., Abbühl, L. M., and Schwab, M.: Erosion-driven uplift of the modern Central Alps, *Tectonophysics*, 474, 236–249, 2009.
- 685 Codilean, A. T.: Calculation of the cosmogenic nuclide production topographic shielding scaling factor for large areas using DEMs, *Earth Surface Processes and Landforms*, 31, 785–794, 2006.
- Cowgill, E.: Cenozoic right-slip faulting along the eastern margin of the Pamir salient, northwestern China, *Geological Society of America Bulletin*, 122, 145–161, 2010.
- Ducea, M. N., Lutkov, V., Minaev, V., Hacker, B. R., Ratschbacher, L., Luffi, P., Schwab, M., Gehrels, G. E.,
690 McWilliams, M., Vervoort, J., and Metcalf, J.: Building the Pamirs: The view from the underside, *Geology*, 31, 849–852, 2003.
- Dunai, T.: *Cosmogenic Nuclides: Principles, Concepts and Applications in the Earth Surface Sciences.*, Cambridge, 2010.
- Fan, G., Nil, J. F., and Wallace, T. C.: Active tectonics of the Pamir and Karakorum, *Journal of Geophysical
695 Research*, 99, 7131–7160, 1994.
- Fuchs, M. C., Gloaguen, R., and Pohl, E.: Tectonic and climatic forcing on the Panj river system during the Quaternary, *International Journal of Earth Sciences*, 102, 1985–2003, 2013.
- Fuchs, M. C., Gloaguen, R., Krbetschek, M. R., and Szulc, A.: Rates of river incision across the main tectonic units of the Pamir identified using optically stimulated luminescence dating of fluvial terraces, *Geomorphology*,
700 216, 79–92, 2014.
- Gabet, E., Burbank, D. W., Pratt-Sitaula, B., Putkonen, J., and Bookhagen, B.: Modern erosion rates in the High Himalayas of Nepal, *Earth and Planetary Science Letters*, 267, 482–494, 2008.
- Gardelle, J., Berthier, E., Arnaud, Y., and Kääh, A.: Region-wide glacier mass balances over the Pamir-Karakoram-Himalaya during 1999–2011, *The Cryosphere*, 7, 1263–1286, doi:10.5194/tc-7-1263-2013, 2013.
- 705 Garzanti, E., Vezzoli, G., Andò, S., Lavé, J., Attal, M., France-Lanord, C., and DeCelles, P.: Quantifying sand provenance and erosion (Marsyandi River, Nepal Himalaya), *Earth and Planetary Science Letters*, 258, 500–515, 2007.
- Godard, V., Lavé, J., Carcaillet, J., Cattin, R., Bourlès, D., and Zhu, J.: Spatial distribution of denudation in Eastern Tibet and regressive erosion of plateau margins, *Tectonophysics*, 491, 253–274, 2010.
- 710 Godard, V., Burbank, D. W., Bourlès, D. L., Bookhagen, B., Braucher, R., and Fisher, G. B.: Impact of glacial erosion on ¹⁰Be concentrations in fluvial sediments of the Marsyandi catchment, central Nepal, *Journal of Geophysical Research*, 117, F03 013, 2012.
- Godard, V., Bourlès, D. L., Spinabella, F., Burbank, D. W., Bookhagen, B., Fisher, G. B., Moulin, A., and Leanni, L.: Dominance of tectonics over climate in Himalayan denudation, *Geology*, 42, 243–246, 2014.
- 715 Granger, D. E., Kirchner, J. W., and Finkel, R.: Spatial averaged long-term erosion rates measured from in situ-produced cosmogenic nuclides in alluvial sediment, *Journal of Geology*, 104, 249–257, 1996.
- Gruber, F. E. and Mergili, M.: Regional-scale analysis of high-mountain multi-hazard and risk indicators in the Pamir (Tajikistan) with GRASS GIS, *Natural Hazards and Earth System Sciences*, 13, 2779–2796, 2013.
- Herber, L. J.: Separation of feldspar from quartz by flotation, *The American Mineralogist*, 54, 1212–1215, 1969.
- 720 Huffman, G. J., Adler, R. F., Arkin, P., Chang, A., Ferraro, R., Gruber, A., Janowiak, J., McNab, A., Rudolf, B., and Schneider, U.: The Global Precipitation Climatology Project (GPCP) Combined Precipitation Dataset, *Bulletin of the American Meteorological Society*, 78, 5–20, 1997.

- Huffman, G. J., Bolvin, D. T., Nelkin, E. J., Wolff, D. B., Adler, R. F., Gu, G., Hong, Y., Bowman, K. P., and Stocker, E. F.: The TRMM Multisatellite Precipitation Analysis (TMPA): Quasi-Global, Multiyear,
725 Combined-Sensor Precipitation Estimates at Fine Scales, *Journal of Hydrometeorology*, 8, 38–55, 2007.
- Huntington, K. W., Blythe, A. E., and Hodges, K. V.: Climate change and Late Pliocene acceleration of erosion
in the Himalaya, *Earth and Planetary Science Letters*, 252, 107–118, 2006.
- Ischuk, A., Bendick, R., Rybin, A., Molnar, P., Khan, S. F., Kuzikov, S., Mohadjer, S., Saydullaev, U., Ilyasova,
Z., Schelochkov, G., and Zubovich, A. V.: Kinematics of the Pamir and Hindu Kush regions from GPS
730 geodesy, *Journal of Geophysical Research: Solid Earth*, 118, 2408–2416, 2013.
- Korschinek, G., Bergmaier, A., Faestermann, T., Gerstmann, U. C., Knie, K., Rugel, G., Wallner, A., Dillmann,
I., Dollinger, G., von Gostomski, C. L., Kossert, K., Maiti, M., Poutivtsev, M., and Remmert, A.: A new value
for the half-life of ^{10}Be by Heavy-Ion Elastic Recoil Detection and liquid scintillation counting, *Nuclear Inst.*
and Methods in Physics Research, B, 268, 187–191, 2010.
- 735 Korup, O.: Earth's portfolio of extreme sediment transport events, *Earth Science Reviews*, 112, 115–125, 2012.
- Korup, O., Densmore, A. L., and Schlunegger, F.: The role of landslides in mountain range evolution, *Geomor-*
phology, 120, 77–90, 2010.
- Koulakov, I. and Sobolev, S. V.: A tomographic image of Indian lithosphere break-off beneath the Pamir-
Hindukush region, *Geophysical Journal International*, 164, 425–440, 2006.
- 740 Lal, D.: Cosmic ray labeling of erosion surfaces: *in situ* nuclide production rates and erosion models, *Earth and*
Planetary Science Letters, 104, 424–439, 1991.
- Lupker, M., Blard, P.-H., Lavé, J., France-Lanord, C., Leanni, L., Puchol, N., Charreau, J., and Bourlès, D.:
 ^{10}Be -derived Himalayan denudation rates and sediment budgets in the Ganga basin, *Earth and Planetary*
Science Letters, 333–334, 146–156, 2012.
- 745 Merchel, S. and Herpers, U.: An update on radiochemical separation techniques for the determination of long-
lived radionuclides via accelerator mass spectrometry, *Radiochim. Acta*, 84, 215–219, 1999.
- Merchel, S., Arnold, M., Aumaître, G., Benedetti, L., Bourlès, D. L., Braucher, R., Alfimov, V., Freeman, S. P.
H. T., Steier, P., and Wallner, A.: Towards more precise ^{10}Be and ^{36}Cl data from measurements at the 10^{14}
level: Influence of sample preparation, *Nuclear Inst. and Methods in Physics Research, B*, 266, 4921–4926,
750 2008.
- Merchel, S., Bremser, W., Akhmadaliev, S., Arnold, M., Aumaître, G., Bourlès, D. L., Braucher, R., Caffee, M.,
Christl, M., Fifield, L. K., Finkel, R. C., Freeman, S. P. H. T., Ruiz-Gómez, A., Kubik, P. W., Martschini,
M., Rood, D. H., Tims, S. G., Wallner, A., Wilcken, K. M., and Xu, S.: Quality assurance in accelerator
mass spectrometry: Results from an international round-robin exercise for ^{10}Be , *Nuclear Inst. and Methods*
in Physics Research, B, 289, 68–73, 2012.
- 755 Mohadjer, S., Bendick, R., Ischuk, A., Kuzikov, S., Kostuk, A., Saydullaev, U., Lodi, S., Kakar, D. M., Wasy,
A., Khan, M. A., Molnar, P., Bilham, R., and Zubovich, A. V.: Partitioning of India-Eurasia convergence in
the Pamir-Hindu Kush from GPS measurements, *Geophysical Research Letters*, 37, L041 737, 2010.
- Molnar, P. and England, P.: Late Cenozoic uplift of mountain ranges and global climate change: chicken or
760 egg?, *Nature*, 346, 29–34, 1990.
- Montgomery, D. R. and Brandon, M. T.: Topographic controls on erosion rates in tectonically active mountain
ranges, *Earth and Planetary Science Letters*, 201, 481–489, 2002.

- Nishiizumi, K., Imamura, M., Caffee, M. W., Southon, J. R., Finkel, R. C., and McAninch, J.: Absolute calibration of ^{10}Be AMS standards, *Nuclear Instruments and Methods in Physics Research, B*, 258, 403–413, 2007.
- 765 Norton, K. P. and Vanacker, V.: Effects of terrain smoothing on topographic shielding correction factors for cosmogenic nuclide-derived estimates of basin-averaged denudation rates, *Earth Surface Processes and Landforms*, 34, 145–154, 2009.
- Norton, K. P., Abbuhl, L. M., and Schlunegger, F.: Glacial conditioning as an erosional driving force in the Central Alps, *Geology*, 38, 655–658, 2010.
- 770 Oumet, W. B., Whipple, K. X., and Granger, D. E.: Beyond threshold hillslopes: Channel adjustment to base-level fall in tectonically active mountain ranges, *Geology*, 37, 579–582, 2009.
- Pohl, E., Knoche, M., Gloaguen, R., Andermann, C., and Krause, P.: The hydrological cycle in the high Pamir Mountains: how temperature and seasonal precipitation distribution influence stream flow in the Gunt catchment, Tajikistan, *Earth Surface Dynamics Discussions*, 2, 1155–1215, doi:10.5194/esurfd-2-1155-2014, <http://www.earth-surf-dynam-discuss.net/2/1155/2014/>, 2014.
- 775 Pohl, E., Gloaguen, R., and Seiler, R.: Variability of winter and summer precipitation in the Pamirs and their effects on hydrology and hazards: Application of a HANTS method to decipher highly variable precipitation time series, *Remote Sensing*, p. 22, under review.
- 780 R Core Team: R: A Language and Environment for Statistical Computing, R Foundation for Statistical Computing, Vienna, Austria, <http://www.R-project.org>, 2013.
- Reigber, C., Michel, G. W., Galas, R., Angermann, D., Klotz, J., Chen, J. Y., Papschev, A., Arslanov, R., Tzurkov, V. E., and Ishanov, M. C.: New space geodetic constraints on the distribution of deformation in Central Asia, *Earth and Planetary Science Letters*, 191, 157–165, 2001.
- 785 Robinson, A. C.: Geologic offsets across the northern Karakorum fault: Implications for its role and terrane correlations in the western Himalayan-Tibetan orogen, *Earth and Planetary Science Letters*, 279, 123–130, 2009.
- Röhringer, I., Zech, R., Abramowski, U., Sosin, P., Aldahan, A., Kubik, P. W., Zöller, L., and Zech, W.: The late Pleistocene glaciation in the Bogchigir Valleys (Pamir, Tajikistan) based on ^{10}Be surface exposure dating, *Quaternary Research*, 78, 590–597, 2012.
- 790 Schaller, M., von Blanckenburg, F., Hovius, N., and Kubik, P. W.: Large-scale erosion rates from in situ-produced cosmogenic nuclides in European river sediments, *Earth and Planetary Science Letters*, 188, 441–458, 2001.
- Scherler, D., Bookhagen, B., and Strecker, M. R.: Tectonic control on ^{10}Be -derived erosion rates in the Garhwal Himalaya, India, *Journal of Geophysical Research: Earth Surface*, 119, 83–105, 2014.
- 795 Schmidt, J., Hacker, B. R., Ratschbacher, L., Konstanze, S. b., Stearns, M., Kylander-Clark, A., Cottle, J. M., Alexander, A., Webb, G., Gehrels, G., and Minaev, V.: Cenozoic deep crust in the Pamir, *Earth and Planetary Science Letters*, 312, 411–421, 2011.
- Schneider, F. M., Yuan, X., Schurr, B., Mechie, J., Sippl, C., Haberland, C., Minaev, V., Oimahmadov, I., Gadoev, M., Radjabov, N., Abdybachaev, U., Orunbaev, S., and Negmatullaev, S.: Seismic imaging of subducting continental lower crust beneath the Pamir, *Earth and Planetary Science Letters*, 375, 101–112, 2013.
- 800

- Schwab, M., Ratschbacher, L., Siebel, W., McWilliams, M., Minaev, V., Lutkov, V., Chen, F., Stanek, K., Nelson, B., Frisch, W., and Wooden, J. L.: Assembly of the Pamirs: Age and origin of magmatic belts from the southern Tien Shan to the southern Pamirs and their relation to Tibet, *Tectonics*, 23, TC4002, 2004.
- 805 Sippl, C., Schurr, B., Yuan, X., Mechie, J., Schneider, F. M., Gadoev, M., Orunbaev, S., Oimahmadov, I., Haberland, C., Abdybachaev, U., Minaev, V., Negmatullaev, S., and Radjabov, N.: Geometry of the Pamir-Hindu Kush intermediate-depth earthquake zone from local seismic data, *Journal of Geophysical Research: Solid Earth*, 118, 1438–1457, 2013.
- Stone, J. O.: Air pressure and cosmogenic isotope production, *Journal of Geophysical Research: Solid Earth*, 810 105, 23 753–23 759, 2000.
- Strahler, A., Muchoney, D., Borak, J., Friedl, M., Gopal, S., Lambin, E., and Moody, A.: MODIS Land Cover Product Algorithm Theoretical Basis Document (ATBD) Version 5.0, pp. 1–59, 1999.
- Strecker, M. R., Frisch, W., Hamburger, M. W., Ratschbacher, L., Semiletkin, S., Zamoruyev, A., and Sturchio, N.: Quaternary deformation in the Eastern Pamirs, Tadjikistan and Kyrgyzstan, *Tectonics*, 14, 1061–1079, 815 1995.
- Stübner, K., Ratschbacher, L., Weise, C., Chow, J., Hofmann, J., Khan, J., Rutte, D., Sperner, B., Pfänder, J. A., Hacker, B. R., Dunkl, I., Tichomirowa, M., Stearns, M. A., Bahram, I., Gadoev, M., Gloaguen, R., Jonckheere, R., Kanaev, E., Minaev, V., Oimahmadoc, I., Rajabov, N., and Stanek, K. P.: The giant Shakh dara migmatitic gneiss dome, Pamir, India-Asia collision zone, 2. Timing of dome formation, *Tectonics*, 32, 1404– 820 1431, 2013.
- Trifonov, V. G.: Late Quaternary tectonic movements of western and central Asia, *Geological Society of America Bulletin*, 89, 1059, 1978.
- von Blanckenburg, F.: The control mechanisms of erosion and weathering at basin scale from cosmogenic nuclides in river sediment, *Earth and Planetary Science Letters*, 237, 462–479, 2005.
- 825 Wolman, J. G. and Miller, J. P.: Magnitude and frequency of forces in geomorphic processes, *Journal of Geology*, 68, 54–74, 1960.
- Zech, R., Abramowski, U., Glaser, B., Sosin, P., Kubik, P. W., and Zech, W.: Late Quaternary glacial and climate history of the Pamir Mountains derived from cosmogenic ^{10}Be exposure ages, *Quaternary Research*, 64, 212–220, 2005.